

Topology optimization of a rowing terminal device for an upper limb prosthesis

Román Calcerrada^{*a}, Alberto Donoso^a, Ernesto Aranda^a, David J. McKeown^b, Francisco Ramos^a

^a*Escuela Técnica Superior de Ingenieros Industrial de Ciudad Real, Universidad de Castilla - La Mancha (UCLM).*

^b*School of Mechanical and Materials Engineering, University College Dublin (UCD).*

Abstract

Prostheses are as old as humans, although current conceptions have progressed far from early designs. The prosthesis world is a field in constant evolution, either aiming to replace or to duplicate parts of the human body. In the last four decades, since the inception of activity-specific prosthesis, the industry of sport prosthetic devices has developed considerably and with an increasing number of sport specific systems available. However, due to the complexity and uniqueness of applications, extensive issues remain unresolved. This work presents a new body-powered sport prosthetic mechanism that allows a person with an unilateral upper limb disability to row. A complete computational analysis of the mechanical properties of the device has been performed using finite element methods. Following this, topology optimization methods were applied to obtain a substantial reduction in device weight while retaining the necessary mechanical strength. This process shows the potential of topology optimization in the design of prosthetic terminal devices, achieving lighter and, hence, cheaper and more competitive mechanisms.

Keywords: sport prosthesis, mechanical terminal device, topology optimization, finite elements analysis

1. Introduction

With the aim to replicate or replace human body parts the domain of prosthesis design is challenging. The design of prostheses has been in constant evolution, with the functionality of early devices improved and expanded by engineering materials and new design tools.

The use of sport prostheses were scarce until the 1970's, with a baseball glove and a bowling attachment [1] being the only devices commercially available.

^{*}Corresponding author

Previous to this, upper limb prostheses design was based on a *one-model-fits-all* philosophy [2], focused on generic systems developed to mimic any action the limbs it was replacing could preform. However, the demand for specific application devices increased with the use of sport as a rehabilitation tool for disabled people. The new concept of *activity-specific prostheses* [3] had begun, enabling the quicker and welcomed development of such devices focused on work and sport. As a result, the last four decades of considerable specific upper limb prosthetic devices development has resulted in several systems available for a range of sports, such as archery, mountain bike, ski, golf, basketball, etc. The creation of TRS in 1979 by Bob Radocy¹, improvements in composites and high endurance resins, the adoption of additive manufacturing in the industry, and the constant advancement of CAD software, among others, have been some key factors in achieving this progress. However, a new promising tool is being introduced in this design field. Topology optimization (TO), which currently is already being used in the development of prostheses internal structures which require osseointegration [4], will play a key role in the future development of sport prostheses.

TO has reached a maturity that it can be considered an integral conceptual tool for structural design. Fundamentally, it solves the problem of distributing a set amount of material within a design space so as to optimize a certain objective function while also satisfying a set of constraints. Since the publication of the pioneering work on this method [5], which was initially conceived for structural design only, the spirit of the TO method has been successfully applied to numerous applications, such as the design of metamaterials, compliant mechanisms and piezoelectric actuators, among others [6]. In this work, we will apply TO techniques to reduce the weight of a sport prosthesis while ensuring the structural/mechanical requirements remain satisfied. This work presents a natural continuation of [7], where a sport prosthesis which allows a person with an unilateral upper limb disability to row was developed. This paper covers the engineering stage of the design process of the prosthetic mechanism. Here, this design will be improved and 3D Finite Elements Analysis (FEA) performed to complement the previous work. Finally, uniquely to any other sport prosthesis design process published up to date, a rigorous lightening process is carried out using TO tools.

There are several works found in the literature investigating sport specific devices [8, 9, 10, 11, 12]. However, the majority consist solely of descriptions of existent devices functionality or clinical aspects based on the qualitative aspects provided by an expert's judgment [13], thus omitting the engineering aspect of design process. Due to the lack of published work regarding the design process for a sport-specific prosthesis, this article and the previous one intend to fill this gap, providing detail of whole process, from the initial approach to the final, optimized, result. The aim is to serve as a reference for the design of future sport prosthetic devices. Even with a significant improvement in their

¹<https://www.trsprosthesis.com/>

availability, it remains a relatively new field with a large number of problems to be solved yet. Therefore, the objective of this work is to computationally analyze and optimize the mechanically powered upper limb terminal device (i.e. without external power source) used as part of prosthesis enabling rowing a person with an unilateral amputation of any severity, which was designed in [7].

The paper is structured as follows: Section 2 will present the problem to be solved and the solution which has been adopted; then, in Section 3 some improvements will be made to the initial device design; after that, in Section 4, the redesigned model will be analysed with FEA and different materials for manufacture considered; in Section 5 the TO model will be developed, and a final optimized model will be presented with its corresponding FEA. Finally, some conclusions will be drawn.

2. Statement of the problem

Sculling, or couple, is a rowing discipline where each rower uses two oars to propelling the boat, one in each hand. It consists of a cyclic motion pattern of the human body to provide an efficient means of force transmission. It can be divided in two main phases: drive and recovery. During the drive phase the rower produces the propulsive power, pulling the oar handles while the blades remain below the waterline, perpendicular (squared) to the water surface. After this phase, the blades are removed from the water and feathered, i.e. longitudinally rotated until they are parallel to the water surface. Then, the recovery phase starts and the rower pushes the oars forward to return to the initial position and to start a new stroke.

There was not a single commercial system which allowed participation in this discipline by a person with an unilateral upper limb disability of any degree, so the mechanism of Figure 1(a) was developed in [7]. It is composed of two parts: i) a terminal device attached to the prosthetic socket, which grasps the oar handle and rotates passively, due to the rotation of the oar itself; and ii) a feathering mechanism, which is added to the boat to connect both oars and to transmit the rotational motion between them. The system is based on the working principle of a leader-follower device: through a cable system placed into the boat, both oars are connected in a way that, when one oar rotates, the other, which is attached to the prosthesis, is compelled to do so. This concept is represented by the coloured arrows of Figure 1(a), which shows the behaviour if any movable part is actuated. This mechanism allows a disabled rower to feather and square both oars with the rotation of one arm and to still perform the remaining movements and produce the required forces that a natural sculling stroke implies.

The terminal device of this prosthetic rowing system is the focus of this work. A detailed view is presented in Figure 1(b), where the nomenclature used for its main components is depicted. The clasp is directly attached to the handle, while the wrist is an intermediate part that restricts the motion range of the different movable parts and serves as a base to join the device to the prosthesis. The clasp can rotate 90° with respect to the wrist, and the back rod end allows

95 the complete device to rotate 5° in radial direction and 50° in ulnar direction. These motions, which are depicted in Figure 1(c), compose the two necessary degrees of freedom of the system to fully develop the rowing stroke.

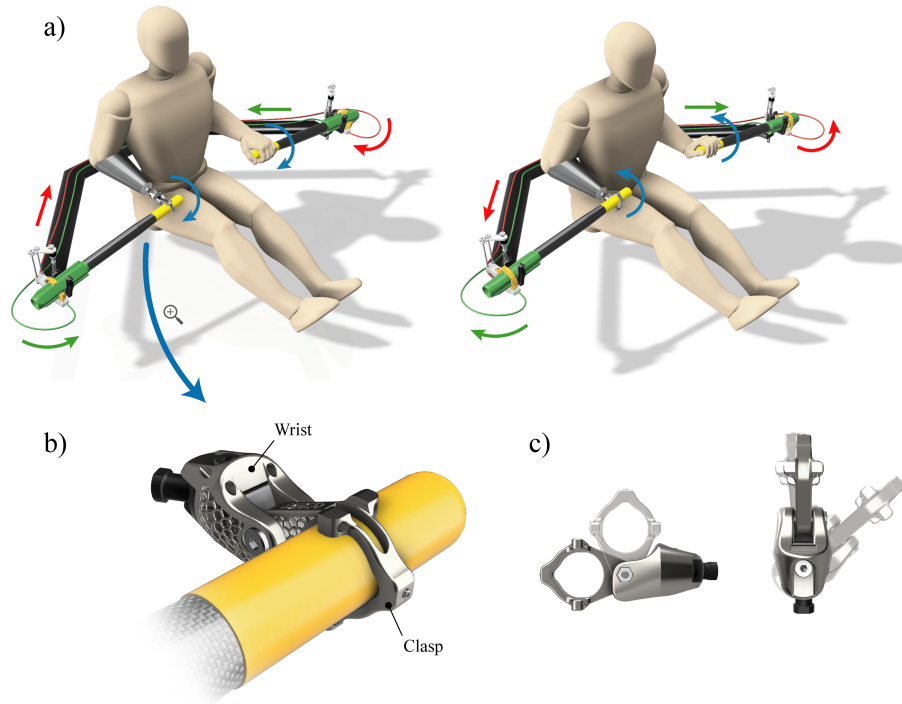


Figure 1: Representation of the prosthetic mechanism designed to allow a person with an unilateral upper limb disability of any severity to row. (a) Complete assembled mechanism solution, which consists in connecting both oars through a cables system placed on the boat, with one oar driven by the able hand and the other attached to the terminal device, to allow feathering and squaring the oar of side with the prosthetic. (b) Detailed view of the terminal device designed to hold the oar. (c) Degrees of freedom and rotation ranges of the terminal device.

Also, it should be noted that for the manufacture of the prosthetic terminal device, due to the complex geometry and the expected low production batch size, additive manufacturing was selected as production technology. In addition, while the system here presented is generic in nature, there might be a need for bespoke user requested changes in, for example, the motion limits of the degrees of freedom. Additive manufacturing allows for quick, low-cost prototypes to be made and the comfort of the device to be quickly tuned.

Hence, any materials discussion will also focus on material printability and the certain additive manufacturing method will depend on the specific selected material, stated down below. Moreover, several prototypes of this mechanism has already been manufactured and not major overhang constraints have been required than the maximum bar thickness allowed by additive manufacturing,

110 which has been considered through the filter radius of the optimization process,
detailed in the subsequent optimization section.

3. Design Improvement stage

Notwithstanding a fully functional terminal device was presented in the pre-
vious work, some of the elements of that first design have been redesigned to
115 solve some design flaws, as not to carry them on to the optimisation stage.
These improvements are compared to the original elements in Figure 2.

Initially, a set screw with plastic tip was placed at the front of the clasp
to secure the oar handle. The design allowed the oar handle slide in and be
tightened in place by the screw. However, the placement of this set screw was
120 a critical point of the clasp, where the highest load was applied. Hence, it
was removed and the tolerance of the handle hole was adjusted to allow simple
press-fit of the rubberised oar handle.

Also, the shoulder bolts used to form the movable joints were replaced by
pins. The shoulder bolts added unnecessary weight and added to design com-
125 plexity. Pins fulfilled the requirement of allowing required degrees of freedom
and smooth relative motion between the parts.

Finally, the initial model was submitted to a manual lightweighting process.
By intuition, material was removed from those parts that were considered struc-
turally irrelevant. However, this weight reduction was removed and the model
130 was returned to its robust shape before being rigorously optimized using TO.

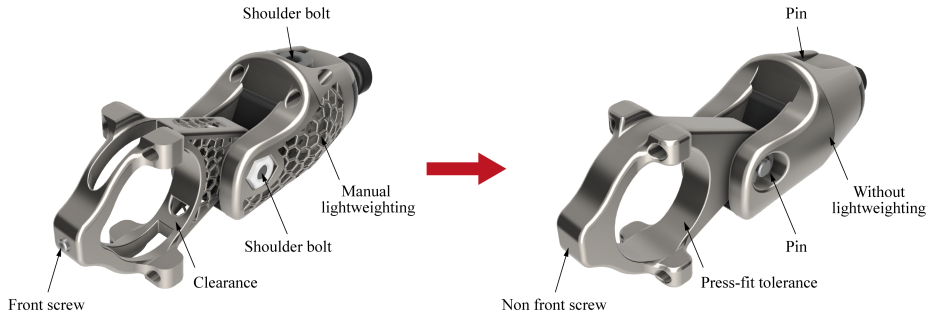


Figure 2: Initial design (left) and improved design without lightweighting (right) of the terminal device.

4. Terminal device FEA

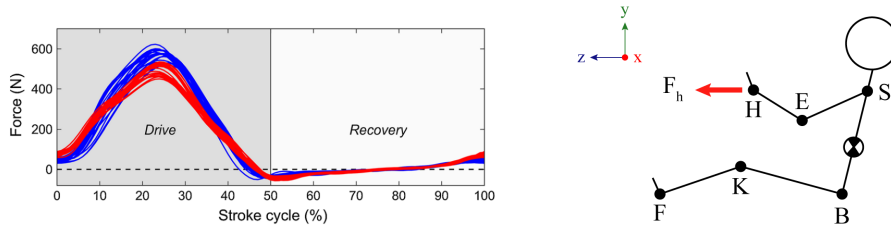
Before doing any TO, a FEA simulations was carried out to provide an
insight of the structural loads on the components and allow assessment of the
viability of TO providing significant improvements. Following this reasoning,
135 FEAs of the separate parts of the terminal device are developed here. The

software used for this analysis is *Autodesk Fusion 360*² (hereinafter Fusion), which integrates Autodesk’s Nastran solver, a robust and trusted FEA tool.

Among the different analysis options that Fusion provides there is a static stress analysis which is used to consider the worst case scenario of each rowing phase (i.e the one with the highest load requirements). It is assumed that if the device is able to bear these load configurations, it will not fail at any other situation.

The main parts of the terminal device, the clasp and wrist, are analysed separately for two different phases of a rowing stroke, the drive and recovery phases shown in Figure 3(a), as [14] suggests. At both stages, the input load, provided by the rower hands and labelled as \mathbf{F}_h in Figure 3(b), is completely horizontal, following [15] criteria.

In summary, four stress analysis are performed. The drive phase and the recovery phase of the clasp and the wrist, respectively. The details of each simulation and the corresponding results are presented in detail below.



(a) Force exerted during recovery and drive phases [14]. (b) Schematic representation of the main force.

Figure 3: Key aspects to determining stroke load state.

4.1. Drive phase

During the drive phase of a sculling stroke, the rower produces the power to propel the boat forward. They do this by pulling backwards on the handles of the oars while the blades remain squared in the water. The worst-case scenario of this phase takes place midway, when there is an average peak load value of 500 N on each hand (1000 N in total) [14, 16], identified as $\mathbf{F}_{h,d}$. At this moment, the rower has their arms completely extended and their hands perfectly aligned with them. For the terminal device this means that the clasp and the wrist are aligned with the athlete’s forearm as well. Figure 4(a) shows the position of all the elements at this moment, which are used to determine the parameters of the FEA simulations.

Clasp

Due to the geometric and structural symmetry of the clasp respect to the plane YZ , only half of the domain was considered for the simulations, reducing the overall computational load. To keep the equivalence with the original

²<https://www.autodesk.com/products/fusion-360>

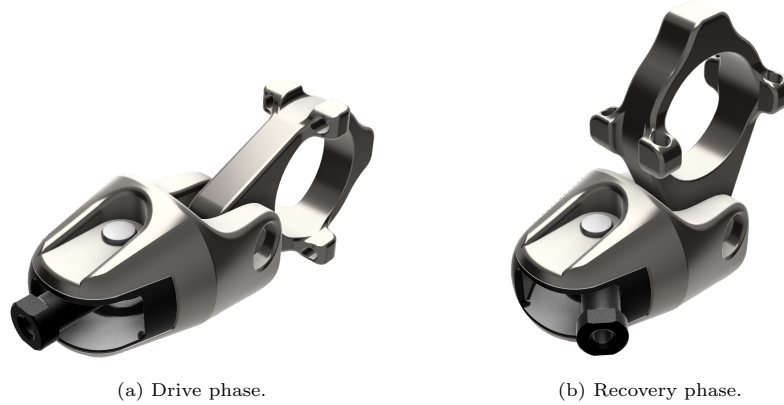


Figure 4: Position of the terminal device in the different rowing phases.

model, a boundary condition which limits the X displacement of the highlighted pink surface of Figure 5(a) was implemented. Another condition constraining the radial displacement of the highlighted blue face of the Figure 5(a), which corresponds to the pin joint between the clasp and the wrist was added.

170 Two different forces were applied as the boundary conditions loads. The first force, $\mathbf{F}_{h,d}$, is the load that the rower exerts when pulling the oar, which is transmitted to the clasp as a reaction force of the handle over its contact surface, the highlighted red face of Figure 5(b). As it is applied on a cylindric surface, a realistic approach is to model this as a bearing load of 250 N module (half of
 175 500 N owing to the symmetry simplification). This is a parabolic distribution load with maximum value at $Y = 0$, decreasing until zero at maximum Y . The second force is the contact force between the clasp and the wrist, identified as \mathbf{F}_s , uniformly applied over the green surface highlighted in Figure 5(b). A magnitude of 25 N was chosen for this load, which has been vectorially decomposed
 180 to being adequately applied to each direction.

The meshing process in Fusion starts from an initial user defined mesh type and size and solves the problem iteratively, gradually reducing the mesh size of the critical zones of the model until convergence is achieved. For this case, parabolic elements with curve capacity and an initial size of 10% model-based
 185 were set, while, for the mesh refinement process, a maximum of 10 iterations with 5% of results tolerance, based on Von Mises stresses, was fixed.

Finally, the material was set to a 3D printable titanium alloy, Ti_6Al_4V [17], but a material selection discussion will be developed based on these results. Stress and deformation results provided by the software are shown in Figure 5(c),
 190 with a 22.2 MPa peak value.

Wrist

As there is not geometrical and structural symmetry in this part, the complete 3D model, without simplifications, was considered. A single displacement

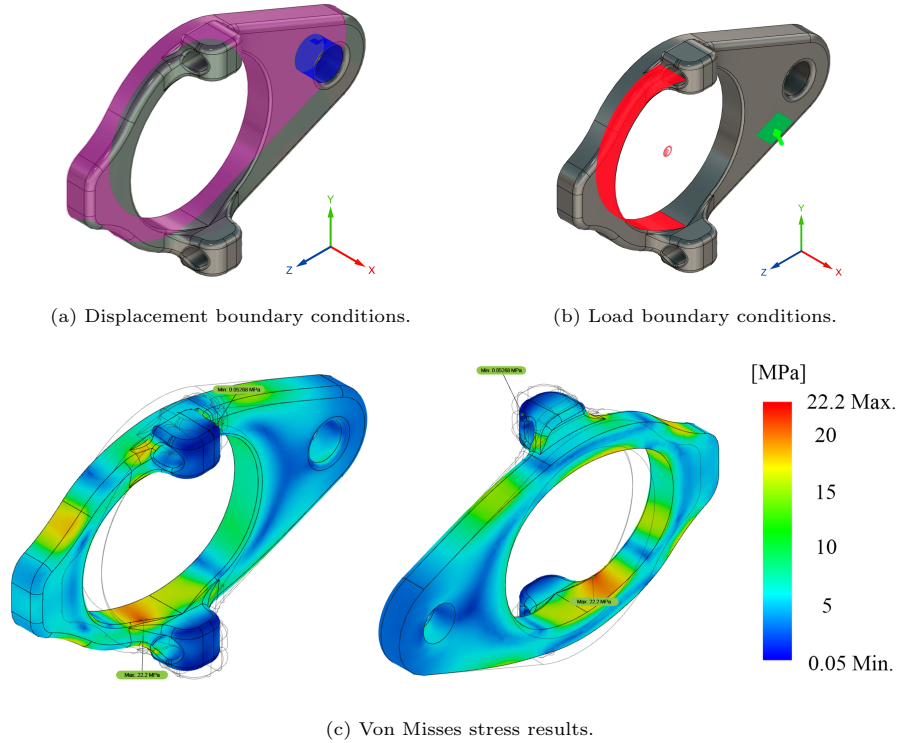


Figure 5: Boundary conditions and results of the clasp during the drive phase.

boundary condition was applied in this case at the pin that joins the wrist and
 195 the rod end. Hence, the radial displacement of the highlighted blue surfaces of
 Figure 6(a) are constrained.

The same forces as the previous case have been applied as the load boundary
 conditions. The first force, the propulsion load, $\mathbf{F}_{h,d}$, is transferred to the wrist
 as the reaction force that the pin joining the clasp exerts on its contact. It has
 200 also been applied as a 500 N module bearing load over the red surfaces of the
 Figure 6(b). The second force, the contact force, \mathbf{F}_s , between the clasp and the
 wrist has also been included. A load of 50 N has been uniformly applied on the
 green surface highlighted in Figure 6(b).

The meshing features and material properties were exactly as the previous
 205 model. Von Mises stress results of the wrist are shown in Figure 6(c), where the
 peak value is 21.5 MPa.

4.2. Recovery phase

The recovery phase of a sculling stroke takes place when the rower moves
 to return to the initial position to commence a new stroke. The rower pushes
 210 the handles of the oars forward while the blades remain feathered out of the
 water. The worst-case scenario of this phase arises in the beginning, when there

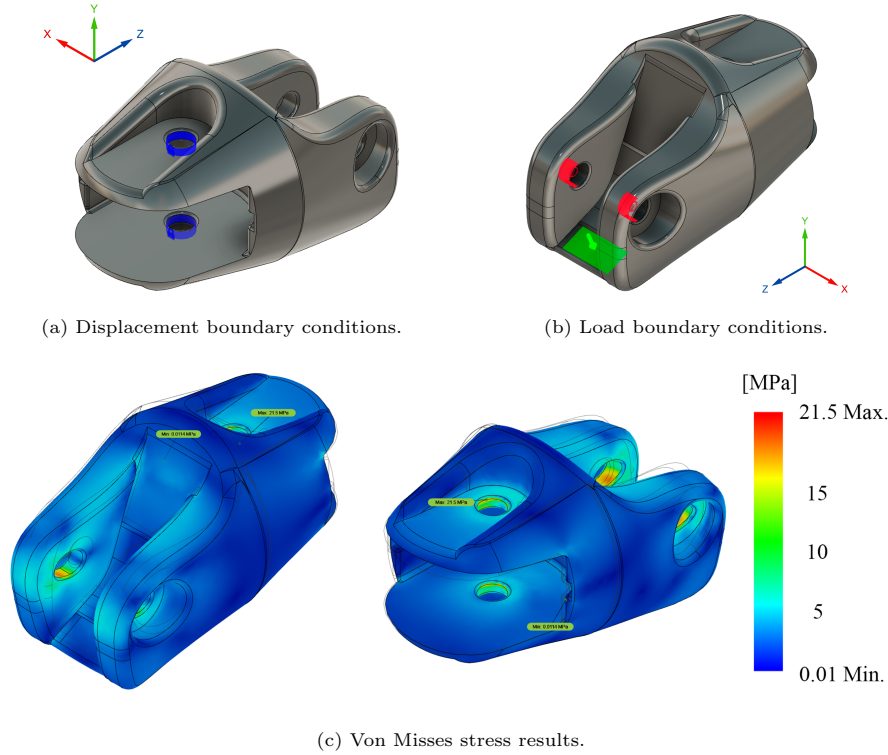


Figure 6: Boundary conditions and results of the wrist during the drive phase.

is a peak load value of 50 N on each hand (100 N in total) [18], denoted as $\mathbf{F}_{h,r}$. At this moment, the rower wrists are bent in such way that the hands form a 90° angle with the forearms to keep the blade parallel to the water surface, and the arms are also flexed so that the wrists are 50° bent in the ulnar direction with respect to the forearms. Hence, the clasp is 90° rotated with respect to the wrist, until they hit the stop, and the rod end is 50° rotated in ulnar direction respect to the wrist, also at the limit of motion, to keep that position. Figure 4(b) shows this terminal device configuration, which will determine the configuration parameters of the FEA simulations.

Clasp

Displacement boundary conditions are identical to the drive phase (Figure 5). There are two loads at the boundary: the load $\mathbf{F}_{h,r}$ of the red surface of Figure 7(a) where the oar is pushed, applied as a bearing load of 25 N module (half of 50 N due to symmetry simplification); and the load \mathbf{F}_s of the green surface of Figure 7(a), that simulates the contact between the clasp and the wrist, of 25 N module, which is uniformly distributed over the green surface.

Von Mises stress results of the numerical simulation of the clasp in the recovery phase are shown in Figure 7(b), where the peak value is 4.63 MPa.

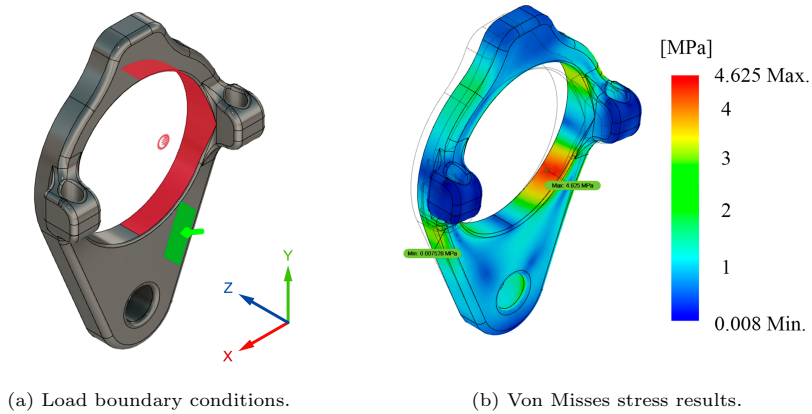


Figure 7: Boundary conditions and results of the clasp during the recovery phase.

230 *Wrist*

As in the drive case, the only displacement boundary condition is applied to the pin that joins wrist and rod end, where the radial displacement of the highlighted blue surfaces of Figure 6(a) are constrained.

235 And with respect to the boundary condition loads, three different forces were applied. The 50 N bearing load of the pushing force, $\mathbf{F}_{h,r}$, transferred to the wrist as the reaction force the pin exerts in the red surfaces of Figure 8(a). The 50 N of the contact load, \mathbf{F}_s , between the clasp and the wrist, uniformly applied in the green surface of Figure 8(a). And the 50 N of the contact load, \mathbf{F}_b , between the rod end and the wrist, also uniformly applied in the yellow surface highlighted in Figure 8(a).

240 The stress results of the wrist in the recovery phase are shown in Figure 8(b), with a peak value of 13.16 MPa.

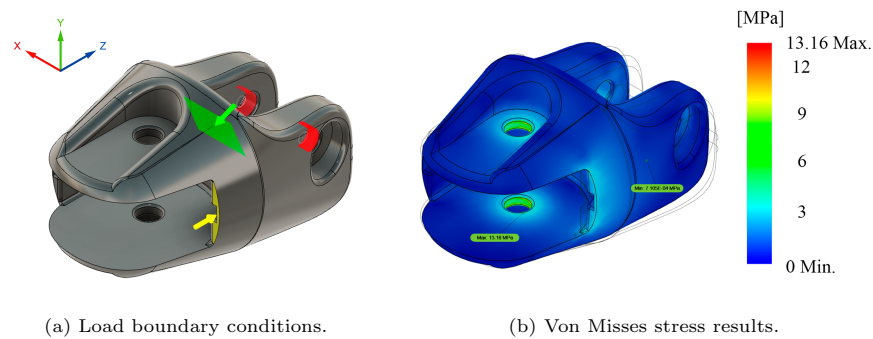


Figure 8: Boundary conditions and results of the wrist during the recovery phase.

Table 1: FEA results of the non-optimized parts of the terminal device.

Phase	Part	Parameter	Ti ₆ Al ₄ V	Rf. nylon	PLA
Drive	Clasp	σ_{MVM} (MPa)	22.20	22.15	22.15
		ε_{max}	$2.77 \cdot 10^{-4}$	$1.25 \cdot 10^{-3}$	$7.84 \cdot 10^{-3}$
		SF	> 15	10.82	3.25
	Wrist	σ_{MVM} (MPa)	21.50	21.40	21.40
		ε_{max}	$3.19 \cdot 10^{-4}$	$1.44 \cdot 10^{-3}$	$9.05 \cdot 10^{-3}$
		SF	> 15	11.21	3.37
Recovery	Clasp	σ_{MVM} (MPa)	4.63	4.63	4.63
		ε_{max}	$6.82 \cdot 10^{-5}$	$3.1 \cdot 10^{-4}$	$1.94 \cdot 10^{-3}$
		SF	> 15	> 15	> 15
	Wrist	σ_{MVM} (MPa)	13.16	13.14	13.14
		ε_{max}	$2.03 \cdot 10^{-4}$	$9.2 \cdot 10^{-4}$	$5.76 \cdot 10^{-3}$
		SF	> 15	> 15	5.5

4.3. Results discussion

The FEA results of every case are shown in Table 1. To assess the structural state of each part, different key parameters have been collected from the simulations: the maximum Von Mises stress, σ_{MVM} ; the maximum strain value, ε_{max} ; and the safety factor, SF .

The safety factor will determine if a model can withstand the corresponding loads and the structural margin before breaking. It is given by

$$SF = \frac{\sigma_0}{\sigma_{MVM}} \quad (1)$$

and relates the yield strength of the material, σ_0 , with the maximum Von Mises stress value. We assume as design criteria that $SF \in [2, 4]$.

The results establish that the Ti₆Al₄V model is oversized in all parts as the safety factor greatly exceeds the design range. As a result, other 3D printable materials have also been studied, namely reinforced nylon with continuous carbon fibres and polylactic acid (PLA). The mechanical properties of any 3D printed material heavily depend on the printing parameters. [19] and [20] have been consulted, respectively, to obtain these properties.

The adoption of either of these two materials allows a substantial cost and weight reduction for the device, while the required structural strength is still guaranteed as FEA results demonstrated. In fact, the results of reinforced nylon model indicate that the design geometry is still oversized, while the results obtained using PLA are within to the design criteria.

Hence, some relevant conclusions can be taken from these results. Using PLA the terminal device would meet the strength criteria. The mechanical properties of the titanium alloy and the nylon reinforced are unnecessarily high for the application, but may offer superior properties when aspects such as high temperature performance and chemical resistance is require. Nevertheless,

there is still room for cost and weight improvement/reduction in all the models through the use of TO methods. PLA model can be lightened, whilst the overall strength of the parts are kept. Also, large amounts of material can be removed from the titanium and reinforced nylon models and still easily meet the design criteria. However, the PLA model is selected as the focus for the topology optimization process.

5. Topology optimization

As it was mentioned in the introduction, the philosophy of the TO method is to find the topology of a structure that optimizes a desired objective function and at the same time satisfies some constraints. In this case, a minimum compliance problem with a volume constraint.

For a given domain Ω , being the reference configuration of a linear isotropic elastic body with boundary $\partial\Omega = \Gamma_D \cup \Gamma_N \cup \Gamma_F$, we try to find a characteristic function χ of a subdomain of Ω where we put the material. If $\sigma(\mathbf{u})$ is the stress given by Hooke's law:

$$\sigma(\mathbf{u}) = 2\mu\varepsilon(\mathbf{u}) + \lambda \operatorname{tr}(\varepsilon(\mathbf{u}))I$$

where $\varepsilon_{ij}(\mathbf{u}) = \frac{1}{2} \left(\frac{\partial u_i}{\partial x_j} + \frac{\partial u_j}{\partial x_i} \right)$ is the linearized strain tensor, and λ and μ are the Lamé coefficients, then the displacement \mathbf{u} of the structure is the solution of the linear elasticity system (*), and the optimization problem is expressed as

$$\begin{aligned} \min_{\chi} J(\chi) &= \int_{\Omega} \mathbf{f} \cdot \mathbf{u} + \int_{\Gamma_N} \mathbf{t} \cdot \mathbf{u} \\ \left. \begin{aligned} -\operatorname{div}(\sigma(\mathbf{u})) &= \mathbf{f} && \text{in } \Omega \\ \mathbf{u} &= \mathbf{0} && \text{on } \Gamma_D \\ \sigma(\mathbf{u}) \cdot \mathbf{n} &= \mathbf{t} && \text{on } \Gamma_N \end{aligned} \right\} (*) \\ \frac{1}{|\Omega|} \int \chi &\leq V_0 \end{aligned}$$

where J is the compliance, which is a measure of the structure's flexibility in terms of the displacements generated by body forces (\mathbf{f}) and boundary forces (\mathbf{t}), and the last inequality corresponds to a volume constraint, where $V_0 \in (0, 1)$ is a given constant (as a percentage of the total volume of the domain).

The role of χ is introduced throughout Young's modulus, in the form

$$E = E_0\chi + E_{\min}(1 - \chi)$$

where E_0 is the Young's modulus of the material, and E_{\min} is a very small value simulating the void to circumvent singularity problems in the elasticity system.

As this problem is mathematically ill-posed, the characteristic function is often replaced by a density function, taking any possible value between 0 (void) and 1 (material) in every point of the domain. This way to proceed in TO

is called a density-based approach, and in particular, here we use the SIMP method (Solid Isotropic Method with Penalization) (cf. [21]) to interpolate the Young modulus between the solid and void phases, as

$$E \equiv E(\rho) = E_0\rho^p + E_{\min}(1 - \rho^p)$$

295 where p is the SIMP penalization parameter.

It is well known that SIMP approach requires of regularization in order to admit optimized solutions. Otherwise it is typical the appearance of numerical instabilities, such as mesh dependency and checkerboard pattern formation. The most widely used regularization is the combination of a density filter and a
300 projection scheme. The goal of the filter is to ensure a length-scale in the solid phase, characterized by a filter radius R . It obtains mesh independent solutions, but at the expense of producing a blurry grey transition between solid and void phases. To reduce these intermediate densities values, a projection method, with a smoothed Heaviside function is used to enforce 0/1 designs.

305 The problem is numerically solved using Toptimiz3D (T3D) [22]. T3D is a free-distribution software can solve different types of TO problems handling general geometries and unstructured meshes. It provides a simple graphical user interface for setting up and solving the TO problem. Once the user has introduced all relevant data, the software generates C++ code, and compiles
310 and runs it without further intervention. It is also able to export the results in VTK format for post processing with ParaView [23].

A number of simulations for the PLA were run considering just the loads configuration of the drive phase. After testing different approaches, based on experimental facts, and due to the high load requirements of this rowing stage, it
315 has been observed that the structural and geometrical features of the resultant optimized model satisfy the requirements of any stage of the rowing.

5.1. Clasp model

The domain and boundary conditions for the optimization of the clasp can be seen in Figure 5. As 3D problems are computationally intensive, only half of the
320 model has been considered, using a mesh of 305679 tetrahedrons. The symmetry condition of Figure 5(a) has been imposed, preventing the X displacement of the highlighted pink face.

The remaining set of boundary conditions of the clasp are the same as those of the FEA of the drive phase that was performed at Section 4.1. In addition,
325 the passive zone of the Figure 9 has been defined to ensure that there will be some material enclosing the pin.

T3D does not implement an automated way of applying different types of loads as Fusion does. It uses load functions of any type (point, linear, surface or volume), which greatly expands the range of loads that can be implemented.
330 Therefore, to model the bearing load $F_{h,d} = (0, 0, f_c)$, the following parabolic distribution function for f_c was considered [24]:

$$F(y) = \frac{F_0}{A} \left[1 - \left(\frac{y}{y_{\max}} \right)^2 \right] \text{ N/m}^2 \quad (2)$$



Figure 9: Passive zone considered in the clasp.

where A is the area, y_{\max} is the limit value of Y coordinate, and F_0 is a constant. This is a pressure load type, a distributed force over a surface, whose value decreases as the absolute value of Y coordinate increases, until it cancels out for the Y limit value.

Then, as the origin of the coordinate system is set on the centre of the handle location, $x \in [-6, 6] \cdot 10^{-3}$, $y \in [-18.6, 18.6] \cdot 10^{-3}$, $A = 3.506 \cdot 10^{-4} \text{ m}^2$ and it is known that the sum value of f_c is 500 N, the magnitude of the force, F_0 , can be computed by integration. Finally, the resultant expression for the Z component of $\mathbf{F}_{\mathbf{h},\mathbf{d}}$ is

$$f_c = 1.68 \left[1 - \left(\frac{y}{0.0186} \right)^2 \right] \cdot 10^6 \text{ N/m}^2 \quad (3)$$

whose evolution is shown in Figure 10(a).

Likewise, as \mathbf{F}_s is a pressure load, it must be explicitly indicated to T3D. So, it is necessary to divide the load components by the implementing area, $4.2 \cdot 10^{-5} \text{ m}^2$. Thus, $F_s = (0, 5.6, 2.3) \cdot 10^5 \text{ N/m}^2$ is the input force for the wrist and clasp contact.

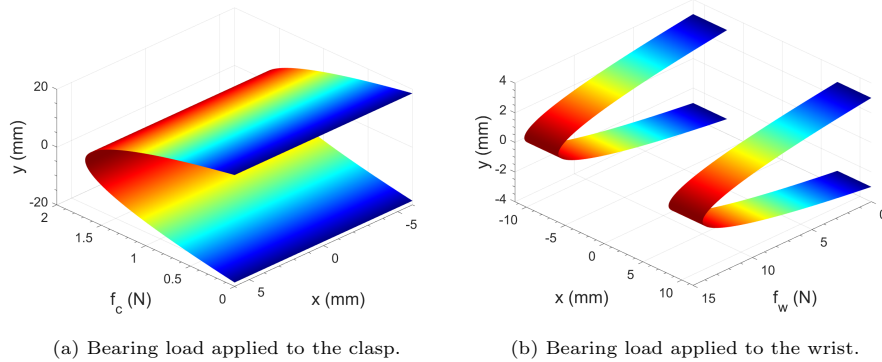


Figure 10: Bearing load distribution implemented in topology optimization.

The volume constraint has been set to $V_0 = 0.65$, i.e. we consider a 65% of the total volume as the maximum volume allowed. This value was determined

by trial and error after several tests removing a significant material amount, checking that the mechanical properties of the structure remained within the design criteria.

Then, a filter radius of 2 mm was chosen to avoid the appearance of extremely thin patterns on the optimized model so that 3D printing manufacturing was feasible (cf. [25, 26]), even with the lowest precision 3D printer of the market. Finally, we selected a Heaviside projection with 4 loops, a SIMP parameter value of 3 and the Method of Moving Asymptotes (MMA, [27]) as a solver. After running the T3D simulation, the resultant model of Figure 11 is obtained.



Figure 11: Topology optimization results of the clasp in PLA.

5.2. Wrist model

For the wrist optimization, the whole domain has been considered, (no symmetries available), and only some fillets of the original shape were removed to avoid meshing problems. A 325610 tetrahedrons mesh has been created for this case.

Boundary conditions are identical to the drive phase FEA simulations shown at Figure 6(b). The bearing load $\mathbf{F}_{\mathbf{n}_d}$ has been applied over the pin contacts and the pressure load $\mathbf{F}_{\mathbf{s}}$ over the clasp contact. Additionally, the passive zones of the Figure 12 have been defined.



Figure 12: Passive zones on the wrist.

Setting the origin of the coordinate system as the middle point between the holes of the pin, parameters of equation (2) are $x \in [7.1, 11.5] \cdot 10^{-3}$, $y \in [-3, 3] \cdot 10^{-3}$, $A = 4.15 \cdot 10^{-5} \text{ m}^2$, and the sum load value applied over each

surface is 250 N. Then, the Z component of the bearing load $F_{h,d} = (0, 0, f_w)$ is

$$f_w = 1.42 \left[1 - \left(\frac{y}{0.003} \right)^2 \right] \cdot 10^7 \text{ N/m}^2 \quad (4)$$

370 and its graphical representation is presented in Figure 10(b).

The pressure load, \mathbf{F}_s , which is distributed over the implementing area, measuring $8.4 \cdot 10^{-5} \text{ m}^2$, results in the input force $F_s = (0, -11.2, -4.6) \cdot 10^5 \text{ N/m}^2$.

Using the same optimization parameters as in the clasp model, the resultant optimized model of the wrist is presented in Figure 13, where 35% of the material
375 has been removed.



Figure 13: Topology optimization results of the wrist in PLA.

One of the weak points of TO is the direct generation of immediately manufacturable models. After the optimization, the primitive shapes that define any part are lost and new ones are not automatically generated. It is possible to develop a smoothing post-process to clean up non-manufacturable parts, but it is essential to enter the information of the primitive shapes in any production
380 machine to properly interpret the motion commands and, thus, fabricate the desired product. Currently, some research groups are already working in solving this drawback, but, up to date, TO can only be used as conceptual design tool: it provides a suggested final shape of the model, but it is the job of the
385 designer to decide which of these geometrical changes will be implemented and how they will be applied through a manual post-process.

In this work, this final step has been completed as follows: a) the TO result was imported in STL format using Fusion; b) the original model was overlapped to be used as a template; and c) the geometrical changes suggested by
390 T3D were added using primitive shapes to keep editable geometric information. The optimized post-processed parts of the rowing sport prosthesis are shown in Figures 14 and 15.

Lastly, the structural state of the final parts was also analysed through FEA simulation as in Section 4. Figures 16 and 17 show that the model fulfills the mechanical requirements and maintains the stresses and the safety factor within
395 the acceptance range.



Figure 14: Final result of the optimized clasp.



Figure 15: Final result of the optimized wrist.

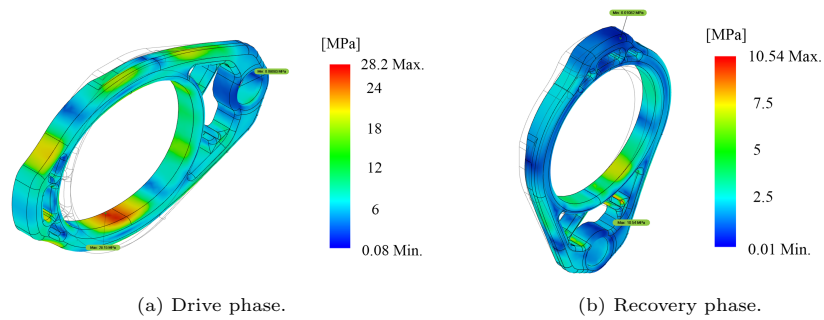


Figure 16: Von Mises stress results of the topology optimized clasp.

6. Conclusions

This paper presented an advanced improvement to the design of an upper limb sport prosthesis for rowing proposed in [7]. Due to the existing gap in the current literature regarding the technical issues involved in the design process of these kinds of systems, we aimed to provide a work flow to serve as a guide for the analysing and optimizing phase of future sport prosthetic devices.

The computational analyses developed through FEA provided a deep insight

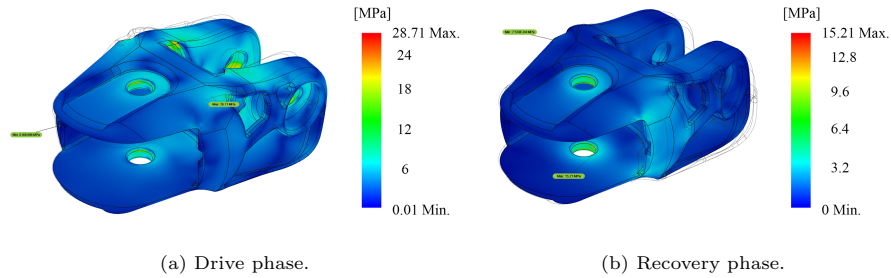


Figure 17: Von Mises stress results of the topology optimized wrist.

of the structural state of the terminal device, which allowed the identification of its strengths and weaknesses. In the light of these results, several changes were performed to the original model.

The implementation of topology optimization techniques enabled a rigorous removal of material, while not violating the mechanical strength requirements for each part. Therefore, a substantial reduction of weight and cost was achieved. Moreover, not only has the potential of topology optimization as a conceptual design tool in the field of external sport prosthesis been proven, but the capability of the free-distribution software Toptimiz3D for optimizing pure 3D parts as well.

Finally, this work provided a workflow to get manufacturable pieces from topology optimization software, (whole process is summarized in Figure 18), and a detailed way of implementing more realistic computational simulations through the use of bearing loads functions.

In the end, it is certain that the availability of sport prostheses has considerably increased in recent years, with several activity-specific assistance systems now commercially available, but in spite of this increase, it is a relatively new sector with problems which are unresolved, especially for people with upper limb disabilities. Hence, we would like to present this work to encourage the development of new prosthetic concepts.



Figure 18: Topology optimization process of the complete terminal device.

7. Acknowledgements

425 Authors acknowledge financial support from the Spanish Ministerio de Ciencia, Innovación y Universidades through grant PID2020-116207GB-I00 and Junta de Comunidades de Castilla - La Mancha through grant SBPLY/19/180501/000110.

References

- 430 [1] J. Cowart, Sport Adaptations for Unilateral and Bilateral Upper-Limb Amputees, *American Alliance for Health, Physical Education and Recreation* 2 (10) (1979).
- [2] R. Radocy, Upper-extremity prosthetics: Considerations and designs for sports and recreation, *Clinical Prosthetics and Orthotics* 11 (3) (1987) 131,153.
- 435 [3] R. Radocy, *Atlas of Limb Prosthetics: Surgical, Prosthetic and Rehabilitation Principles*, 2nd Edition, American Academy of Orthopedic Surgeons, 2002, Ch. 12C, Special Considerations: Upper-Limb Prosthetic Adaptations for Sports and Recreation.
- 440 [4] T. Jansari, I. Deiab, Comparative study of a topologically optimized lower limb prosthesis, *International Journal on Interactive Design and Manufacturing (IJIDeM)* 13 (2) (2019) 645–657.
- [5] M. P. Bendsøe, N. Kikuchi, Generating optimal topologies in structural design using a homogenization method, *Comput. Methods Appl. Mech. Engng.* 71 (2) (1988) 197,224.
- 445 [6] M. P. Bendsøe, O. Sigmund, *Topology optimization: theory, methods, and applications*, 2nd Edition, Springer, 2003.
- [7] D. J. McKeown, R. Calcerrada, F. Ramos, Design of a mechanical upper limb sport prosthesis for rowing, submitted (2022).
- 450 [8] A. Tiele, S. Soni-Sadar, J. Rowbottom, S. Patel, E. Mathewson, S. Pearson, D. Hutchins, J. Head, S. Hutchins, Design and development of a novel upper-limbcycling prosthesis, *Bioengineering* 4 (2017).
- [9] M. J. Highsmith, S. L. Carey, K. W. Koelsch, C. P. Lusk, M. E. Maitland, Kinematic evaluation of terminal devices for kayaking with upper extremity amputation, *Journal of Prosthetics and Orthotics* 1919 (3) (2007) 84,90.
- 455 [10] R. Radocy, *Care of the Combat Amputee*, Office of the Surgeon General, United States Army ; Borden Institute, Walter Reed Army Medical Center : For sale by the Supt. of Docs., U.S. G.P.O., 2010, Ch. 24, Upper Limb Prosthetics for Sports and Recreation, pp. 641,668.

- 460 [11] D. Netland, D. Barlow, L. Fay, M. Morton, A. Burkhardt, Adaptive Technology Catalog , Tech. rep., James Madison University, last accessed 15-07-2020 (2008).
- [12] Hosmer, Upper extremity, product catalog (2012).
- [13] M. Bragaru, R. Dekker, J. H. Geertzen, Sport prostheses and prosthetic adaptations for the upper and lower limb amputees: an overview of peer reviewed literature, *Prosthetics and Orthotics International* 3 (63) (2012).
465
- [14] J. Warmenhoven, S. Cobley, C. Draper, R. Smith, Over 50 years of researching force profiles in rowing: What do we know?, *Sports Medicine* 48 (12) (2018) 2703,2714.
- [15] D. Cabrera, A. Ruina, V. Kleshnev, A simple 1+ dimensional model of rowing mimics observed forces and motions, *Human Movement Science* 25 (2) (2006) 192,220.
470
- [16] B. Elliott, A. Lyttle, O. Birkett, The rowperfect ergometer: A training aid for on-water single scull rowing, *Sports biomechanics, International Society of Biomechanics in Sports* 1 (2002) 123,134.
- 475 [17] K. Karolewska, B. Ligaj, M. Wirwicki, G. Szala, Strength analysis of ti6al4v titanium alloy produced by the use of additive manufacturing method under static load conditions, *Journal of Materials Research and Technology* 9 (2) (2020) 1365,1379.
- [18] G. Marcolin, A. Lentola, A. Paoli, N. Petrone, Rowing on a boat versus rowing on an ergo-meter: A biomechanical and electromyographycal preliminary study, *Procedia Engineering* 112 (2015) 461,466.
480
- [19] J. Chacón, M. Caminero, E. García-Plaza, P. Núñez, Additive manufacturing of pla structures using fused deposition modelling: Effect of process parameters on mechanical properties and their optimal selection, *Materials & Design* 124 (2017) 143,157.
485
- [20] J. M. Chacón, M. A. Caminero, E. García-Plaza, I. García-Moreno, J. M. Reverte, Additive manufacturing of continuous fibre reinforced thermoplastic composites using fused deposition modelling: Effect of process parameters on mechanical properties, *Composites Science and Technology* 181 (8) (2019).
490
- [21] M. P. Bendsøe, Optimal shape design as a material distribution problem, *Structural Optimization* 1 (4) (1989) 193,202.
- [22] E. Aranda, J. Bellido, A. Donoso, Toptimiz3d : a free-distribution software for structural optimization, *Advances in Engineering Software* 148 (2020) 1–10.
495

- [23] U. Ayachit, *The ParaView Guide: A Parallel Visualization Application*, Kitware, Incorporated, 2015.
- [24] Robert C. Juvinall, Kurt M. Marshek, *Fundamentals of Machine Component Design*, 5th Edition, Jonh Wiley & Sons, Inc, 2012.
- 500 [25] B. Tymrak, M. Kreiger, J. Pearce, Mechanical properties of components fabricated with open-source 3-d printers under realistic environmental conditions, *Materials & Design* 58 (2014) 242,246.
- [26] W. Wu, P. Geng, G. Li, D. Zhao, H. Zhang, J. Zhao, Influence of layer thickness and raster angle on the mechanical properties of 3d-printed peek and a comparative mechanical study between peek and abs, *Materials* 8 (9) 505 (2015) 5834,5846.
- [27] K. Svanberg, The method of moving asymptotes—a new method for structural optimization, *International Journal for Numerical Methods in Engineering* 24 (2) (1987) 359,373.